Electronic Supplementary Material (ESI) for Energy & Environmental Science.

Supporting Information

TIN/VANADIUM REDOX ELECTROLYTE COMBINING BATTERY-LIKE ENERGY STORAGE CAPACITY WITH SUPERCAPACITOR-LIKE POWER HANDLING

Juhan Lee,[a,b] Benjamin Krüner,[a,b] Aura Tolosa,[a,b] Sethuraman Sathyamoorthi,[a,c] Daekyu Kim,[a,d] Soumyadip Choudhury,[a] Kum-Hee Seo,[d] and Volker Presser[a,b,*]

[a] INM – Leibniz Institute for New Materials, Campus D2 2, 66123 Saarbrücken, Germany

[b] Department of Materials Science and Engineering, Saarland University, Campus D2 2, 66123 Saarbrücken, Germany

[c] Electrochemical Process Engineering Division, CSIR-Central Electrochemical Research Institute, Karaikudi, 630 006, India

[d] School of Energy, Materials and Chemical Engineering, Korea University of Technology and Education, Chungjeol-ro 1600, 31253 Cheonan, Republic of Korea

* Corresponding author's eMail: volker.presser@leibniz-inm.de

Standard redox potential of various elements

Standard redox potential of various redox couples are shown in **Figure S1**: the potential values are taken from Ref [1]. The oxygen evolution potential described in **Figure 1D** is determined according to the pH value of the 0.75 M $SnSO_4$ / 2 M $VOSO_4$ aqueous solution (pH = 0.63) obtained by SG2-SevenGo pH-Meter (Mettler Toledo).

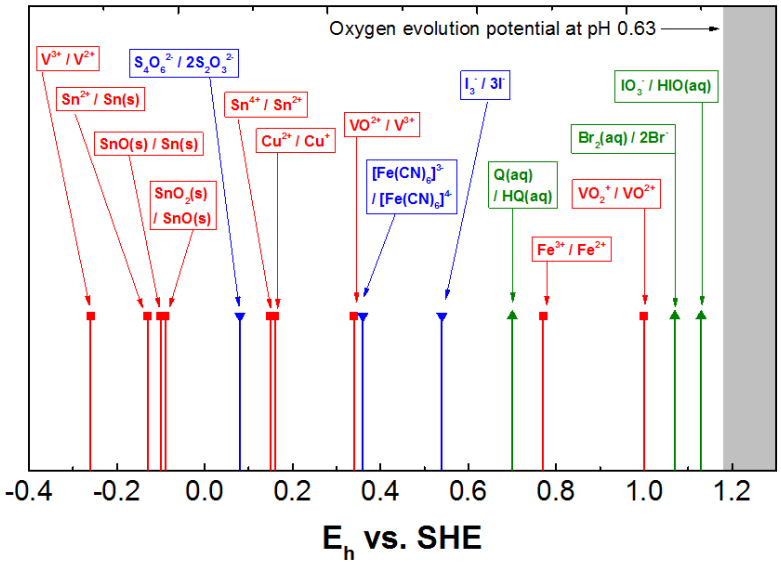

Figure S1: Standard redox potentials of various redox couples which can be applied to redox electrolyte hybrid system.

Membrane treatment, cell assembly and cell configurations for the electrochemical analysis

Anion exchange membranes (FAS15) were provided by FuMA-Tech with the dry thickness of 14±1 µm as measured by a digital micrometer caliper. In order to activate the as-received FAS15 membranes, the membranes were soaked in deionized water for 8 h, then for at least 72 h in 0.5 M H_2SO_4 solution while changing the electrolyte with fresh electrolyte more than three times. We also applied a porous separator (Merck Milipore) made of PTFE with dry thickness of 25 µm in order to characterize the electrochemical performance of the double-layer capacitors in 1 M H_2SO_4 and 1 M Na_2SO4 aqueous solution for comparison.

In case of a full-cell without employing a reference electrode, a particular cell was designed (**Figure S2A**) which allowed the complete sealing of the ion exchange membrane and to limit the excess volume of the redox electrolyte; here, excessive volume means the volume of the electrolyte in the cell except the geometrical volume of the film electrode. For the cell assembly, the redox electrolyte was dropped to the gasket channel having a size of 1.33 cm^2 where the circular film electrode with the same size (1.13 cm^2) was placed, and the cell was tightly sealed afterward.

For the utilization of the Ag/AgCl reference electrode, a spring-loaded two-piston cell (**Figure S2B**) was applied. Even though this cell design does not allow the complete sealing of the ion exchange membrane, the redox shuttling kinetic was reduced into a significantly low level allowing the short term measurement (<1 h) with the negligible influence of redox shuttling.

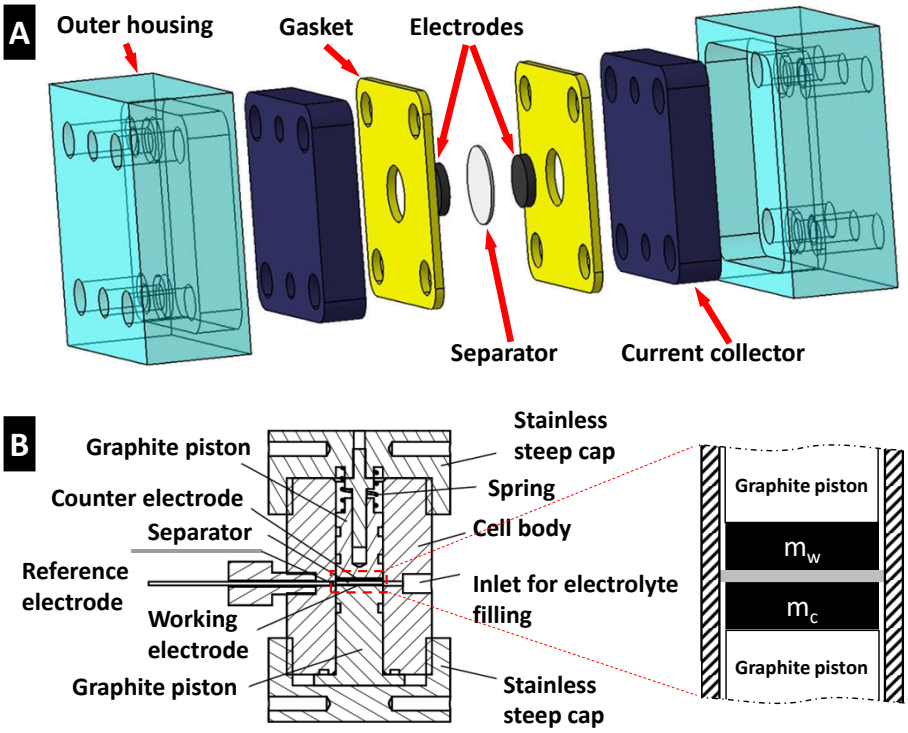

Figure S2: Design of the cells applied for the electrochemical analysis (A-B). (A) Exploded-view drawing of the full-cell without excess volume of electrolyte via gasket sealing for the limited amount of the electrolyte. (B) Schematic illustration of the cell with excess volume of electrolyte. Inset shows the mass of the working electrode (m_w) and the counter electrode (m_c).

In case of measuring the individual potential profile of the positive and negative electrodes in the full-cell (**Figure 1SB**) with a galvanostatic charge and discharge mode, symmetric film electrodes with a diameter of 10 mm were placed between graphite current collectors while being separated by FAS15 membrane. With the aid of the reference electrode, the potential of the counter electrode was measured vs. Ag/AgCl while the potential of the cell was controlled through the potential difference between the positive and the negative electrode (**Table S1**). In case of a half-cell configuration, an electrode with a diameter of 4 mm was applied as working electrode while placing a counter electrode with ca. 38 mg that is more than 30 times larger mass than that of working electrode. Through this mass overbalance, the potential range at the counter electrode was relatively smaller than the applied potential range at the working electrode which allowed to investigate the redox activity at the working electrode without the influence of the redox reactions at the counter electrode (**Figure S3**).

Table S1: Different wire configurations for the potentiostat /galvanostat were applied for the cell in redox electrolytes with a reference electrode. Working electrode potential (U_w) and counter electrode potential (U_C) were controlled or measured either by GCPL or cyclic voltammetry.

Type	U_W	U_C	m_w	m_C
Full-cell	working vs. counter	counter vs. reference	7 mg	7 mg
Half-cell	working vs. reference	counter vs. reference	1.1 mg	38 mg

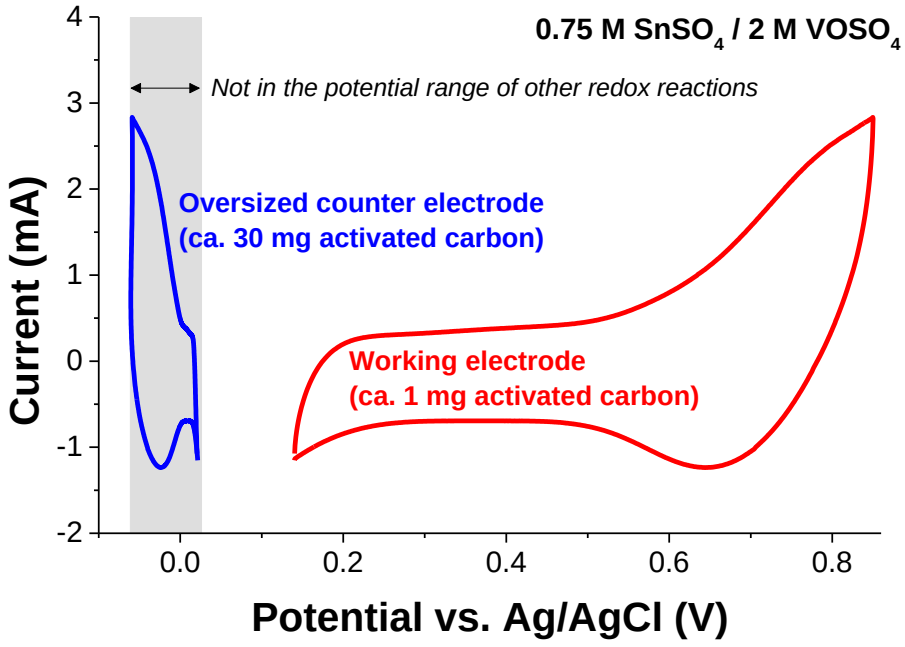

Figure S3: Cyclic voltammogram of a half-cell was obtained for the investigation of the redox activities at the working electrode by minimizing the potential range of the counter electrode via mass overbalance. In case of 0.75 M $SnSO_4$ / 2 M $VOSO_4$ system, the potential range of the counter electrode was not in the range of the other possible redox reactions.

Electrochemical characterization

For the electrochemical characterizations, a VMP300 potentiostat/galvanostat (Bio-Logic) was used while keeping the temperature at 25 °C. For the normalization of the specific energy (*E*), specific power (*P*), and specific current, the total mass of activated carbon material is considered to provide a comparative data basis with battery and supercapacitor materials in the literature. Specific energy was calculated by *Eq. S1* and *Eq. S2*.

$$E_{CV} = \frac{1}{m_{total}} \cdot \int U i_{CV}\, dt \tag{S1}$$

$$E_{GC} = \frac{i}{m_{total}} \cdot \int U\, dt \tag{S2}$$

where E_{CV} is the energy density calculated from cyclic voltammetry, U is the applied voltage, i_{CV} is the measured current, m_{total} is the total mass of the active carbon material in a full-cell, E_{GC} is the energy density calculated from galvanostatic charge and discharge mode, and i is the applied current. The specific power of the full-cell was derived by dividing the specific energy from galvanostatic discharge (E_{GC}) by discharging time (Δt_{dis}) at each specific current step via *Eq. S3*.

$$P = \frac{E_{GC}}{\Delta t_{dis}} \tag{S3}$$

To determine the voltage stability window, S-value test (see Ref. [2]) was performed by cyclic voltammetry (CV) extending the voltage range of the full-cell (**Figure S2A**) from 0.5 V to 1.6 V with the potential interval of 0.5 V at 1 mV·s^{-1}. From the cyclic voltammograms, the S-value were calculated according to the following *Eq. S4*:

$$S = \frac{Q_{char}}{Q_{dis}} - 1 \tag{S4}$$

where Q_{char} is the charge accumulated during charging, Q_{dis} is the recovered charge during discharging.

To condition the cell before the rate handling characterization of the full-cell (**Figure S2A**), a cyclic voltammetry was initially carried out at 1 mV·s^{-1} for 10 cycles at the voltage from 0 V to 1.4 V before further characterization was done. In case of cyclic voltammetry, scan rates from 1 mV·s^{-1} to 2.5 V·s^{-1} were applied for 3 cycles at each scan rate at the voltage from 0 V to 1.4 V. Subsequently, galvanostatic charge/discharge with potential limitation (GCPL) was performed at 50 mA g^{-1} to 30 A g^{-1} with the voltage range from 0 V to 1.2 V or 1.4 V. Afterwards, open circuit voltage measurements over 10 h were carried out after the cell had been discharged to 0 V for 30 min, then, a constant specific current of 400 mA g^{-1} was applied to the cell up to 1.4 V and held at that voltage for 5 h. For the long term cyclic stability test, a galvanostatic cyclic test was applied to the full-cell at 1 A g^{-1} at the voltage window of 1.4 V. For the floating test, symmetric full-cells were charged at 500 mA g^{-1} up to 1.4 V; after that the potential was kept to 1.4 V for 250 h while measuring capacitance for every 10 h by applying 3 cycles in GCPL mode at 500 mA g^{-1} at the voltage window of 1.2 V.

In case of the full-cell with the reference electrode (**Table S1**), the cell was charged by applying a potential from 0 V to 1.4 V between the negative and the positive electrode at 1 A g^{-1} while measuring the potential difference between the negative and the reference electrode. Initially, the cell was stabilized over 20 cycles at 1 A g^{-1}.

In case of the half-cell with the reference electrode (**Table S1**), the cyclic voltammograms of working electrode were measured at a scan rate of 1 mV·s^{-1}.

Electrochemical performance of the $SnSO_4$ / $VOSO_4$ system

For the conditioning of the cell before the S-value characterization, a cyclic voltammetry was initially carried out at 1 $mV \cdot s^{-1}$ for 20 cycles at the voltage from 0 V to 1.4 V. In case of 0.75 M $SnSO_4$ / 2 M $VOSO_4$ system, a very high stability of the electrolyte was observed from the S-value results (**Figure S4C**) which perhaps originate from the high overpotential of metallic tin against hydrogen evolution.

While most of the studies on the $SnSO_4$ / $VOSO_4$ system were carried out with a graphite current collector, we also carried out control experiments with a 100 µm thick platinum current collector (**Figure S4D**) in order to investigate the possible contribution of graphite current collector for the additional energy storage. As characterized at a low scan rate (1 $mV \cdot s^{-1}$), no noticeable difference could be found in the cyclic voltammograms obtained from platinum and graphite current collectors.

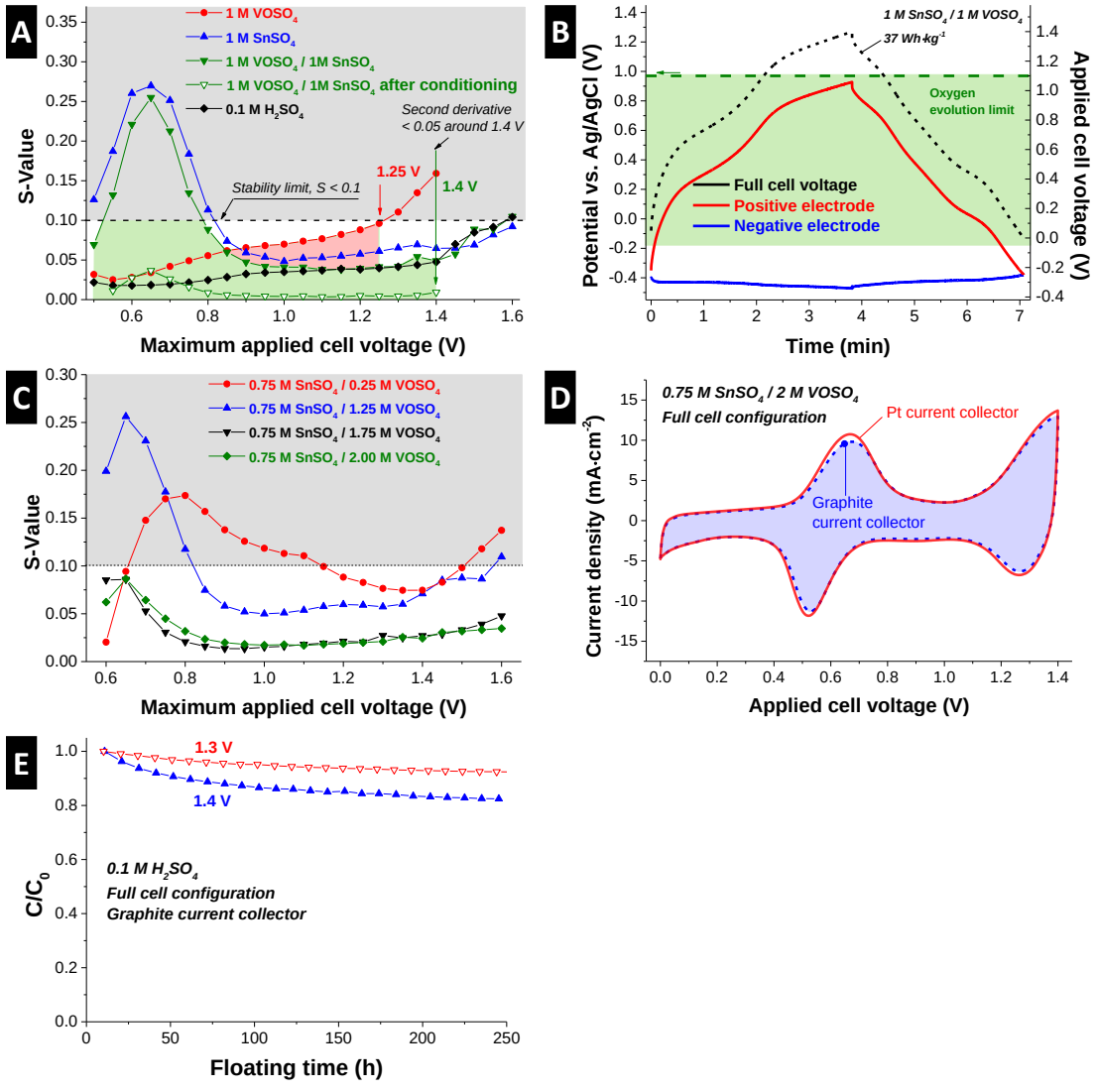

Figure S4: S-Value analysis with various redox electrolytes (A, C). (A) For the conditioning of the 1 M $VOSO_4$ / 1 M $SnSO_4$ cell, initial cyclic voltammograms were applied before the S-Value analysis. (B) Potential profile of the full-cell, the positive, and negative electrode from 1 M $SnSO_4$ / 1 M $VOSO_4$ system by applying a galvanostatic charge and discharge at 1 $A \cdot g^{-1}$. (D) Cyclic voltammogram obtained from a full-cell with 0.75 M $SnSO_4$ / 2 M $VOSO_4$ aqueous solution at 1 $mV \cdot s^{-1}$ by applying graphite current collectors or platinum current collectors. (E) The stability of 0.1 M H_2SO_4 aqueous solution is evaluated by floating test via potential holding at 1.3 V and 1.4 V with symmetric full-cell configuration. The measured capacitance values were normalized to the initial capacitance (C_0).

Structural and chemical analysis

Changes in the morphology of the electrodes were examined by a JEOL JSM 7500F field emission scanning microscope (FE-SEM). The electrodes were fixed with sticky carbon tape on steel sample holder. The composition of the electrodes before and after electrochemical characterization was measured by energy dispersive X-ray spectroscopy (EDX) using a X-Max-150 detector from Oxford Instruments attached to the SEM chamber. Using an accelerating voltage of 10 kV and an emission current of 10 µA, the spectra of 10 different particles was measured. According to the EDX results, the electrode before electrochemical testing contained 0.021±0.004 mole of oxygen per mole of carbon. The electrode with post mortem analysis at -0.2 V showed the increased oxygen and tin content to 0.14±0.03 mole and 0.061±0.004 mole per mole of carbon, respectively.

XPS measurements of the electrode samples were carried out using a K-Alpha+ spectrometer (Thermo Scientific) by applying an Al-K_α mono-source (power: 30 W; spot diameter: 200 µm). For the mounting, the samples were attached to the carbon tape and stayed in the chamber until the vacuum was reached below 10^{-8} mbar before the measurements. The spectra of the samples were obtained in constant analyzer energy mode with a pass energy of 50 eV. The device was calibrated through Au $4f_{7/2}$, Cu $2p_{3/2}$, and Ag $3d_{5/2}$ lines from copper, gold, and silver. For the ion milling, Ar ion beam (4000 eV, 180 s) was applied for etching with the depth of approximately 1-2 µm.

Raman spectra were recorded with a Renishaw InVia Raman system using a laser with a 532 nm excitation wavelength and 0.5 mW power on the sample with a spectral resolution of ca. 1.2 cm^{-1}, using a 50x objective (numeric aperture: 0.9). Raman spectra were recorded with 10 seconds acquisition time using 10 accumulations. The spectra of 15 different points were measured for each side of electrode, the side in contact with the current collector and the side in contact with the ionic exchange membrane. Peak analysis and peak fitting were performed assuming four Voigt peak fitting between 500 and 2000 cm^{-1}.

X-ray diffractograms were collected with a Bruker D8 Discover diffractometer with a LYNXEYE detector using Cu-K_α radiation (0.154 nm) with a step size of 0.02°. The electrodes were placed on a sapphire single crystal to avoid reflexes of the substrate. The system was calibrated with an alumina standard.

The nitrogen gas sorption analyses were carried out with a Quantachrome Autosorb iQ system. For the post mortem analysis, electrode samples were collected after charging the full-cell (**Figure S2A**) to 1.4 V or discharging to 0 V in chronoamperometry mode for 30 min. Afterwards, the negative electrode samples were soaked in 0.1 M H_2SO_4 aqueous solution for a day after the cell disassembly, subsequently soaked into deionized water for a day, and dried in a desiccator in order to remove the dissolved ions. Next, the samples were degassed at 150 °C for up to 20 h at a relative pressure of 0.1 Pa to remove volatile molecules from the surface. The nitrogen sorption analysis was performed in liquid nitrogen at -196 °C. The relative pressure with nitrogen was $5 \cdot 10^{-7}$ to 1.0 in 76 steps. The pore size distribution (PSD) was derived using the quenched-solid density functional theory (QSDFT), assuming slit-like pores.[3-5] The specific surface area (SSA) was also calculated using the Brunauer-Emmett-Teller equation (BET) in the linear regime of the measured isotherms, typically $3 \cdot 10^{-2}$ to $2 \cdot 10^{-1}$ (relative pressure),[6] with a Quantachrome Autosorb 6B. All calculations were performed with the ASiQwin-software 3.0. The evaluated values are summarized in **Table S2**.

The pore size distribution shown in **Figure S5C** shows that the pore size distribution in the range of 0.5-1 nm was not much influenced after the electrochemical conditions of the electrodes. In order to see the clear trend, the d*V*/d*d* values were normalized to peak value around 0.9 nm assuming that the pores in that range were not influenced by the electrochemical treatment (**Figure S5D**). The normalized values indicate that the reduced negative electrode at the cell voltage of 1.4 V might have less pore volumes particularly in the pore size range from 1.2 nm to 3 nm as compared to the pristine electrode made of activated carbon.

Table S2: Summary of the nitrogen gas sorption analysis from the negative electrodes and the pristine electrode made of YP80 type activated carbon and PTFE binder. The post mortem analysis was applied to full-cells exposed to a cell voltage of 1.4 V or 0 V.

Type	SSA_{BET} ($m^2 \cdot g^{-1}$)	SSA_{DFT} ($m^2 \cdot g^{-1}$)	Total pore volume ($cm^3 \cdot g^{-1}$)
YP80 + 5 mass% PTFE	2094	1662	1.05
Post mortem, 1.4 V (full-cell)	1130	981	0.55
Post mortem, 0 V (full-cell)	1783	1520	0.90

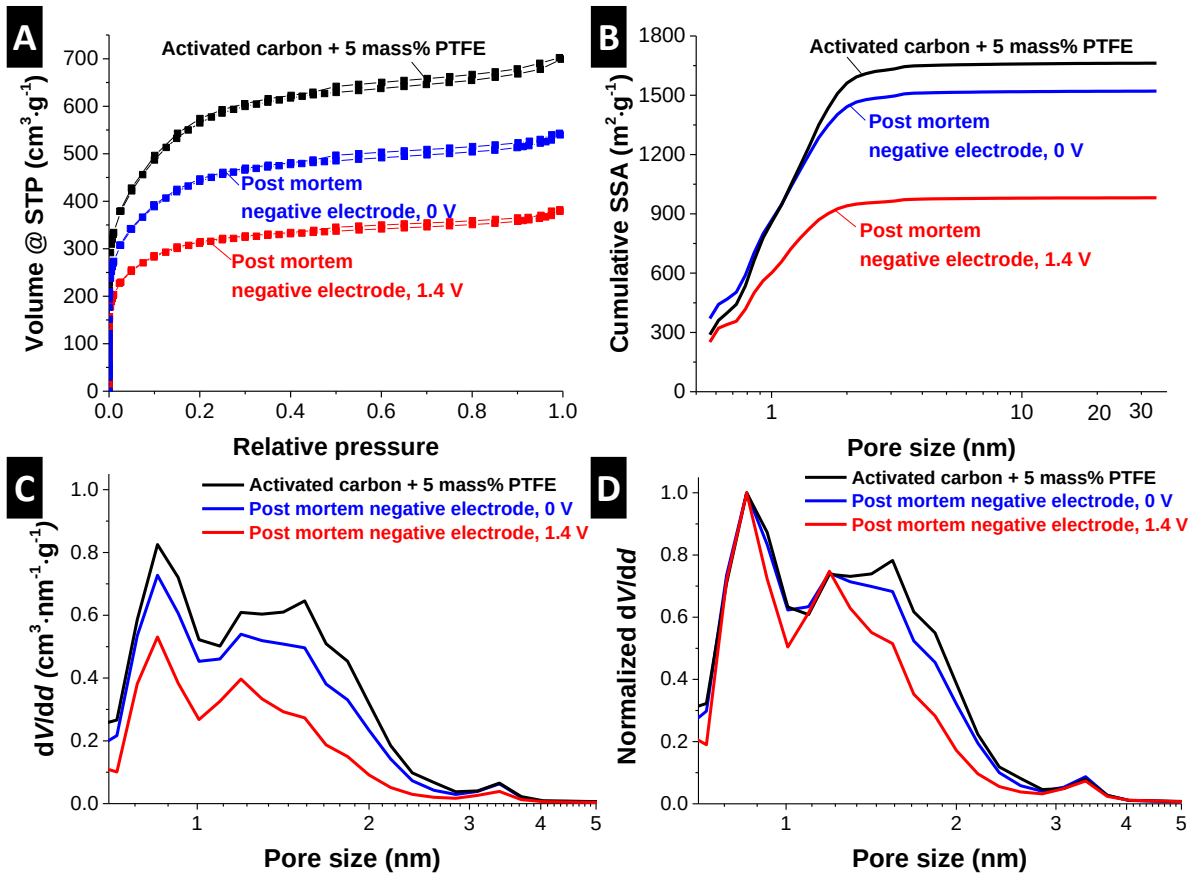

Figure S5: (A-B) Results from post mortem nitrogen gas adsorption analysis. (A) Nitrogen gas sorption isotherms obtained at -196 °C normalized to the total electrode mass and the volume calculated at standard temperature and pressure (STP). (B) Cumulative specific surface area. (C) Pore size distribution calculated by applying the quenched solid density functional theory with slit shape pore model. (D) d*V*/d*d* values are normalized to the peak value obtained in the pore size range 0.5-1 nm.

Tin fluoride formation

The as-prepared activated carbon electrode bound with 5 mass% PTFE, presents a clear F 1s peak of the polytetrafluoroethylene (PTFE) compared to the electrode sample with post mortem analysis at-0.57 V (**Figure S6B**), which shows an extremely small peak for PTFE and a huge peak for metal fluoride. The metal fluorine peak can be identified as SnF_2.

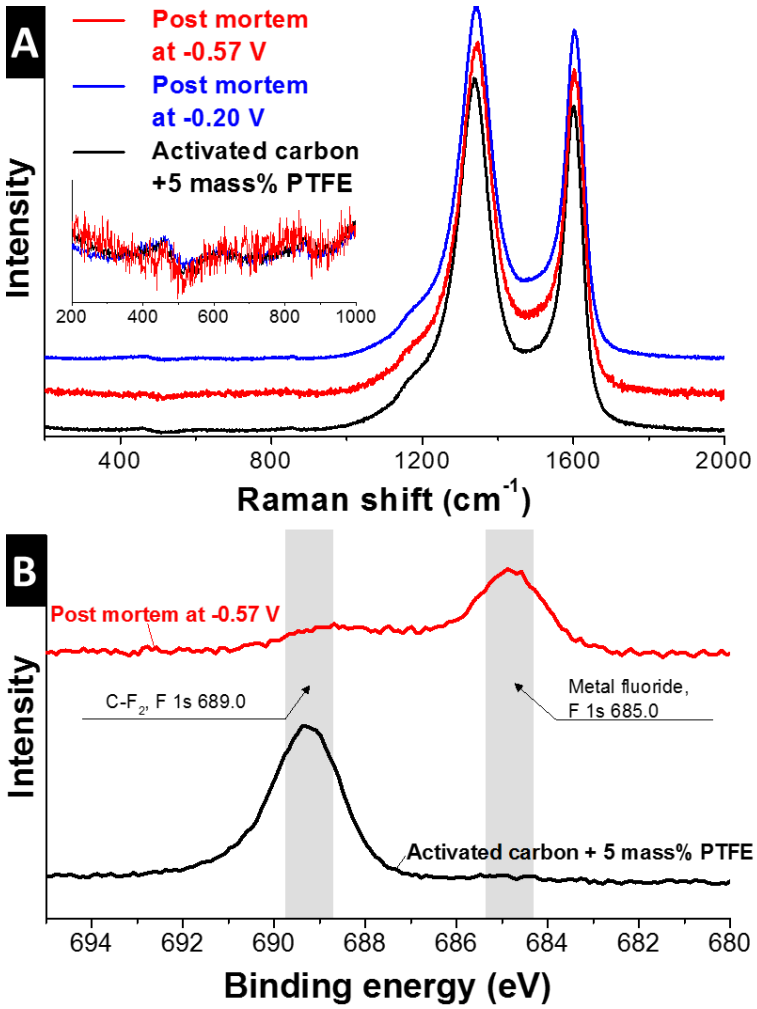

Figure S6: (A) Raman spectra of electrodes before and after electrochemical testing, the inlet shows the Raman spectra between 100 cm^{-1} and 1000 cm^{-1}, wavelength range at which crystalline SnO_2 presents active modes [7]. However due to the amorphous character, this peaks cannot be distinguished from the background. (B) XPS spectra show metal fluoride formation and the weakening of the C-F_2 binding signal for the negative electrode with post mortem analysis at -0.57 V.

Rate handling performance of the $SnSO_4$ / $VOSO_4$ system plotted as a Ragone diagram

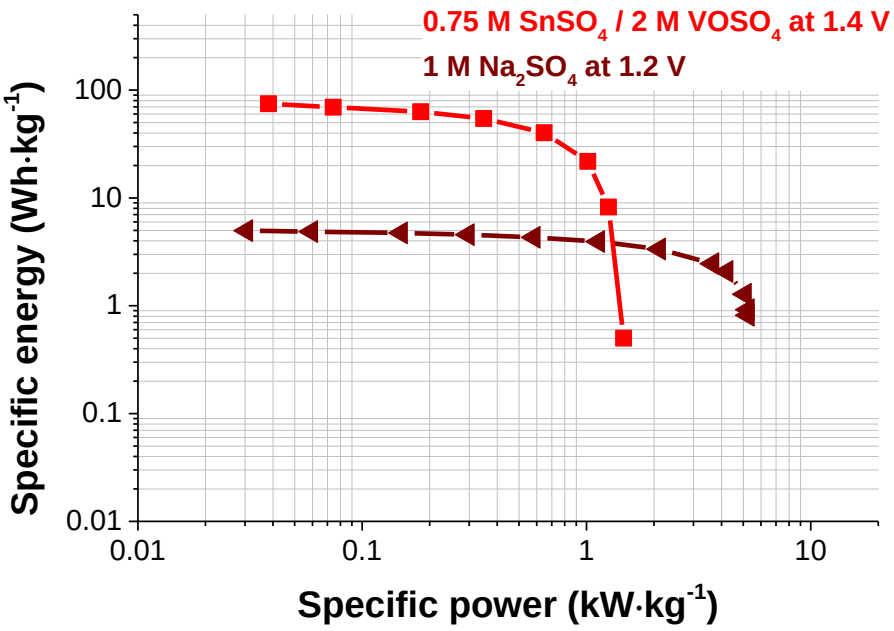

Figure S7: The rate performance of 1 M Na_2SO_4 at 1.2 V and 0.75 M $SnSO_4$ / 2 M $VOSO_4$ at 1.4 V are plotted in a Ragone chart.

Supporting references

[1] B. Averill, P. Eldredge, General chemistry: principles, patterns, and applications, 2011.
[2] D. Weingarth, H. Noh, A. Foelske-Schmitz, A. Wokaun, R. Kötz, Electrochim Acta, 103 (2013) 119-124.
[3] V. Presser, J. McDonough, S.-H. Yeon, Y. Gogotsi, Energ Environ Sci, 4 (2011) 3059.
[4] G.Y. Gor, M. Thommes, K.A. Cychosz, A.V. Neimark, Carbon, 50 (2012) 1583-1590.
[5] A. Vishnyakov, P.I. Ravikovitch, A.V. Neimark, Langmuir, 15 (1999) 8736 - 8742.
[6] S. Brunauer, P.H. Emmett, E. Teller, Journal of the American Chemical Society, 60 (1938) 11.
[7] J. Zuo, C. Xu, X. Liu, C. Wang, C. Wang, Y. Hu, Y. Qian, Journal of applied physics, 75 (1994) 1835-1836.